Unexpected Improved Performance of ALD Coated $LiCoO_2$/Graphite Li-Ion Batteries

Yoon Seok Jung, Peng Lu, Andrew S. Cavanagh, Chunmei Ban, Gi-Heon Kim, Se-Hee Lee, Steven M. George, Stephen J. Harris, and Anne C. Dillon**

The performance of Al_2O_3 atomic layer deposition (ALD) coatings for $LiCoO_2$/natural graphite (LCO/NG) batteries is investigated, where various permutations of the electrodes are coated in a full battery. Coating both electrodes with ~1 nm of alumina as well as coating only the LCO (positive electrode) enables improved performance when cycling at high voltage, where the LCO is known to degrade. However, we found that coating *only* the NG (negative electrode) also improves the performance of the whole battery when cycling at high voltage. Under these conditions, the uncoated LCO (positive electrode) should degrade quickly, and the NG should be unaffected. A variety of characterization techniques show the surface reactions that occur on the negative electrode and positive electrode are related, resulting in the enhanced performance of the uncoated LCO.

1. Introduction

In order to curtail CO_2 production and dependency on limited fossil fuel supplies, lithium-ion batteries (LIBs) are critical to enable electric vehicles e.g. plug-in hybrid electric vehicles (PHEVs) and fully electric vehicles (EVs).[1–3] Although LIBs are the battery of choice for portable electronics, significant challenges must be overcome to enable widespread commercialization of large-format technologies (including both stationary and vehicular applications).[4] The limited electrochemical window of current organic electrolytes, as well as degradation of electrodes at high potential, limits deployment of LIBs in large-scale applications. Specifically, the interfacial stability between the electrodes and electrolyte must be improved in order to achieve long-term stability while also meeting safety requirements.[1,2,5–8] Previously, stabilization of the electrode surfaces has been achieved by using electrolyte additives[9] and surface coatings[10–12] with metal oxides, phosphates, etc. deposited via conventional wet-chemical methods such as sol–gel techniques.

Recently, our group demonstrated atomic layer deposition (ALD) as an advanced coating method for a variety of LIB electrodes[7,8,13–15] and a polymeric separator,[16] which leaded to much attention and the following researches.[17,18] ALD utilizes sequential and self-limiting surface reactions that enable tailored conformal coatings with Å-level thickness control.[19,20] The ability to achieve Å-level control is becoming increasingly important as nanoparticles are now employed in LIBs to achieve high-rate capability, dictating the need for thin coatings.[13,14] An additional advantage of ALD is that it may be employed for both powders and also directly on fully fabricated electrodes.[7,8] Al_2O_3 ALD coatings have already been demonstrated to improve the performance of various positive electrode ($LiCoO_2$[7,13]) and negative electrode (graphite,[8] MoO_3,[14] Fe_3O_4,[15] Si[17]) materials. Specifically, we demonstrated that ultrathin ALD coatings enable significantly improved durability and safety, which we attribute to improved interfacial[7,8,13] and mechanical[14] stability. Unfortunately, true fundamental mechanistic understanding was not previously obtained.

In a significant fraction of Li-ion battery literature, results are obtained from half-cells (HCs), where Li metal is used as the counter/reference electrode to obtain information about the electrode of interest. Although the experiments using the HC (positive electrode/Li or negative electrode/Li) provide an easy

Dr. Y. S. Jung, Dr. C. Ban, Dr. G.-H. Kim, Dr. A. C. Dillon
National Renewable Energy Laboratory
Golden, CO 80401, USA
E-mail: ysjung@unist.ac.kr; Anne.Dillon@nrel.gov
Prof. Dr. Y. S. Jung
Interdisciplinary School of Green Energy
Ulsan National Institute of Science and Technology (UNIST)
Ulsan 689-798, South Korea
Dr. P. Lu, Dr. S. J. Harris
General Motors Research and Development Center
Warren, MI 48090, USA
Dr. A. S. Cavanagh
Department of Physics
University of Colorado at Boulder
Boulder, CO 80309-0215, USA
Prof. Dr. S.-H. Lee
Department of Mechanical Engineering
University of Colorado at Boulder
Boulder, CO 80309-0215, USA
Prof. Dr. S. M. George
Department of Chemistry and Biochemistry and Department of Chemical and Biological Engineering
University of Colorado at Boulder
Boulder, CO 80309-0215, USA

DOI: 10.1002/aenm.201200370

way to estimate the capacity of negative electrodes and positive electrodes separately, in many cases negative results are encountered when a complete battery or full-cell (FC) is fabricated. For example, depletion of lithium from the positive electrode and/or electrolyte may result in gradual capacity loss during repeated cycling, also apparent as <100% Coulombic efficiency.[21] Also, for the well-known spinel $LiMn_2O_4$ positive electrode, $LiMn_2O_4$ is known to suffer from Mn^{2+} dissolution.[22] The Mn^{2+} ions from the positive electrode then migrate through the electrolyte to the negative electrode surface, and are reduced/deposited at a potential of ~1 V (*vs.* Li/Li^+). Then, a fresh solid electrolyte interphase (SEI) film is formed further on the reduced Mn deposits, resulting in degradation of the negative electrode.[23] Surprisingly, by applying an Al_2O_3 coating only to the negative electrode (NG), we found that the positive electrode (LCO) can be stabilized at high voltage in a full battery (or LCO/NG FC configuration). We studied this phenomenon using various characterization techniques including: a unique cell testing configuration, electrochemical impedance spectroscopy (EIS), ex-situ X-ray photoemission spectroscopy (XPS) and time of flight secondary ion mass spectrometry (TOF-SIMS) to achieve mechanistic understanding of this unexpected phenomena.

2. Results and Discussion

In this work, four permutations of LCO/NG FCs were assembled using bare (*b*) or Al_2O_3 ALD coated (*c*) LCO and/or NG electrodes: *b*-LCO/*b*-NG, *b*-LCO/*c*-NG, *c*-LCO/*b*-NG, *c*-LCO/*c*-NG. The well-known ALD process utilizing TMA and H_2O as precursors shown below was employed directly on LCO and NG composite electrodes.[7,8,19]

$$AlOH^* + Al(CH_3)_3 \rightarrow AlO - Al(CH_3)_2^* + CH_4 \quad (1)$$

$$AlCH_3^* + H_2O \rightarrow Al - OH^* + CH_4 \quad (2)$$

Ultrathin Al_2O_3 coating layers were deposited on LCO with 2 cycles of ALD (~2-3 Å) and 5 cycles of ALD on NG following an NO_2/TMA pretreatment (~5-8 Å). From our previous works using the HCs,[7,8,13] the optimized cycle numbers of ALD were chosen in terms of conformality and Li^+ ion transport through the Al_2O_3 coating layers. In case of NG electrode,[8] the NO_2/TMA pretreatment is necessary to ensure a conformal coating on the basal planes of graphitic materials.[24]

Figure 1 displays the cycling performance of four permutations of LCO/NG FCs cycled between 3.25-4.45 V at 0.1C (14 mA g_{LCO}^{-1}) for the first two cycles and 1C (charge/discharge in one hour) for the subsequent cycles at room temperature. The aggressive cycling conditions, with the high upper cut-off potential of 4.45 V, were chosen intentionally to induce severe side reactions on the LCO surface.[7,10,11] (These conditions would have no obvious impact on the NG electrode.) As expected, the *c*-LCO/*c*-NG and the c-LCO/*b*-NG showed superior performance compared to the *b*-LCO/*b*-NG full cell. Also as shown in the Supporting Information (Table S1), *c*-LCO/*c*-NG exhibits negligible capacity fade for 300 cycles with a high initial discharge capacity of ~152 mA h g_{LCO}^{-1} at 0.1C, first two cycles, and subsequent cycles at 1C. We note, the initial discharge

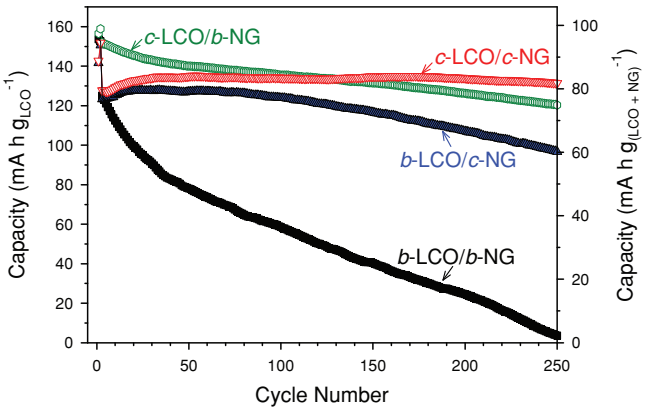

Figure 1. Cycling performance of $LiCoO_2$/natural graphite (LCO/NG) full cells coated with ALD Al_2O_3. Reversible discharge capacity as a function of cycle number for four permutations of LCO/NG cells: Uncoated or bare electrodes are labeled with *b*, and ALD Al_2O_3 coated electrodes are labeled with *c*. Cycling tests were carried out between 3.25–4.45 V at 0.1C for the first two cycles and 1C for subsequent cycles at room temperature.

capacity of a commercially available LCO/NG battery is only ~131 mA h g_{LCO}^{-1} with a voltage cut-off of 4.2 V.[25] Thus, the stable superior capacity of the *c*-LCO clearly demonstrates the protective role of the Al_2O_3 ALD coating to minimize undesirable side reactions and/or dissolution for the positive electrode (with the high voltage cutoff of 4.45 V), as shown previously with LCO/Li HCs.[7] The somewhat inferior performance of *c*-LCO/*b*-NG to that of *c*-LCO/*c*-NG may be attributed to either slightly poorer durability of *b*-NG than *c*-NG and/or more rapid loss of Li^+ due to side reactions on the *b*-NG surface rather than the *c*-NG. Surprisingly, however, the *b*-LCO/*c*-NG performance is only somewhat inferior to that of *c*-LCO/*c*-NG. This behavior is highly unanticipated because uncoated LCO should degrade quickly under such aggressive cycling conditions, cycling up to 4.45 V.[7,10,11] Also our previous HC *b*-NG work showed that *b*-NG loses only ~20% of its initial capacity after 200 room temperature cycles, and the NG is not expected to be affected by the increased upper voltage.[8] Finally, in sharp contrast, ~80% capacity loss is observed for the *b*-LCO/*b*-NG FC after 200 cycles (Figure 1), which is consistent with our expectation that the dominant contribution to failure comes from *b*-LCO. Hence, we must unravel why the c-NG improves the performance of the whole battery.

In order to analyze the situation more fully we measured the potentials of the LCO and NG electrodes separately using a unique three-electrode LCO/Li/NG cell (Figure S1). The potentials of LCO and NG *vs.* Li/Li^+ for *b*-LCO/*b*-NG (dashed line) and *b*-LCO/*c*-NG (solid line) for the first charge at 0.1C are shown in **Figure 2**a, and the same data are shown for the third charge at 1C in Figure 2b. We note first that the plateau at ~0.7–0.8 V (arrow), indicative of electrolyte decomposition,[8] is present on *b*-NG but not on *c*-NG (Figure 2a). We also see that at higher C-rate (1C, Figure 2b), the voltage profile of *c*-NG is negatively shifted (polarized) compared with that of *b*-NG, which may be due to poor Li-ion conductivity of the Al_2O_3 ALD layer. As a result, for the same potential difference between the positive and negative electrodes, the upper cut-off potential *vs.* Li/Li^+

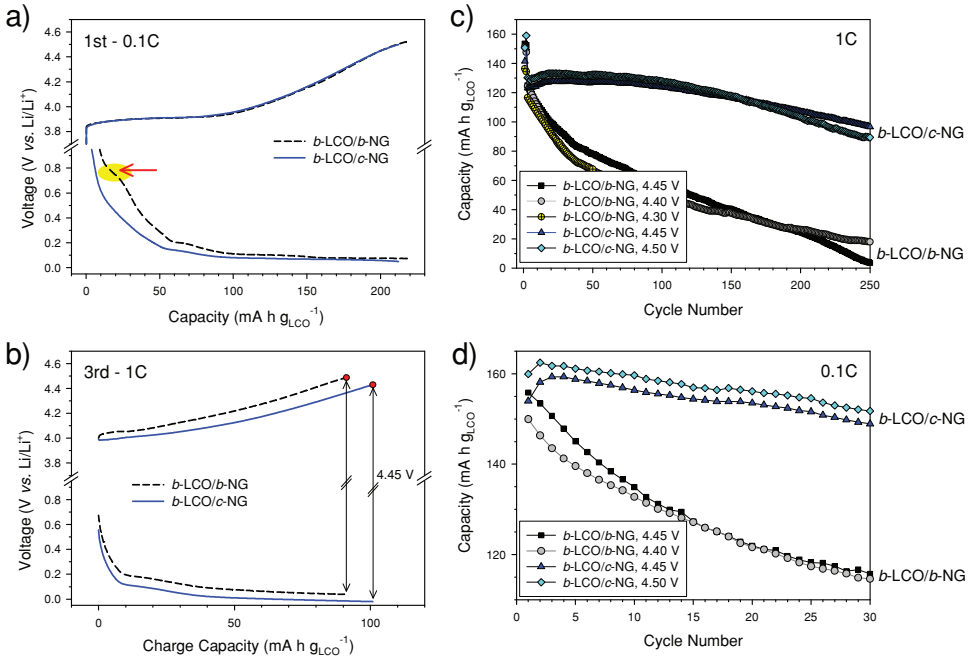

Figure 2. Comparison of electrochemical characteristics between *b*-LCO/*b*-NG and *b*-LCO/*c*-NG full cells. Charge voltage profiles versus Li/Li^+ of *b*-LCO/Li/*b*-NG and *b*-LCO/Li/*c*-NG three electrode cells (a) at 0.1C for the first cycle and (b) at 1C for the third cycle. Note the plateau at ~0.75 V (arrow) associated with the electrolyte decomposition appears on *b*-NG while it does not on *c*-NG for the first cycle in (a). Cycling performances of *b*-LCO/*b*-NG and *b*-LCO/*c*-NG full cells while varying the upper cut-off potential at 0.1C for the first two cycles and (c) 1C for subsequent cycles and (d) 0.1C for all cycles.

of *b*-LCO in the *b*-LCO/*c*-NG cell is lowered by up to 0.06 V at 1C. To evaluate the impact of this polarization, we compared the performance of *b*-LCO/*b*-NG cycled using lower upper cut-off potentials (4.40V and 4.30 V) with *b*-LCO/*c*-NG using an increased upper cut-off potential (4.50 V). The durable capacity tests depicted in Figure 2c show that the *b*-LCO/*c*-NG couple dramatically outperforms the *b*-LCO/*b*-NG couple irrespective of the upper cut-off potential. These results confirm that the 0.06 V change in the upper cut-off potential in the FC does not explain the unexpected benefit of coating the NG electrode. Similarly, the results at 0.1C in Figure 2d where the polarization effect is negligible, also prove that better performance of *b*-LCO/*c*-NG compared with *b*-LCO/*b*-NG is irrespective of the upper cut-off potential.

In order to then assess the degradation of LCO and NG separately, the LCO and NG electrodes, from the cycled LCO/NG FCs, were cut in half and reassembled as LCO/LCO and NG/NG symmetric cells (SCs).[26] Ex-situ EIS experiments on these SCs then allowed us to evaluate the performance of the negative electrode (NG) and positive electrode (LCO) separately, while also removing possible irrelevant signals from the reference Li metal electrode.[27] **Figure 3**a shows a Voigt-type equivalent circuit model[28] comprised of resistors (R), capacitors (C), and a Warburg term (W). Nyquist plots of LCO/LCO and NG/NG SCs, reassembled from the four permutations of FCs, are shown in Figures 3b–e and 3f–i, respectively. An example of the data and the fitting results from an equivalent circuit shown in Figure 3a is displayed in the Supporting Information (Figure S2). Examining the semicircles for *b*-LCO cells (Figure 3b, c), and comparing them to those of *b*-NG cells (Figure 3f, h), it is obvious that those of the *b*-NG are much smaller. Also for the *b*-NG the growth after cycling is negligible, indicating negligible increase in resistance. Furthermore, the semicircles for *c*-NG cells (Figure 3g, i) become smaller after cycling (suggesting a few cycles maybe necessary to reduce the resistance of the coated electrode). We may therefore easily conclude that there is no significant degradation for *b*-NG, and that the unusual improvement in cycling the FC upon coating the NG is not primarily due to enhanced performance of the NG electrode. However, it is extremely interesting that the size of the semicircle of *b*-LCO in the *b*-LCO/*c*-NG cell ('^' in Figure 3c) is dramatically smaller than that of the *b*-LCO/*b*-NG cell ('#' in Figure 3b), still suggesting a correlation between coating the NG and decreased degradation of the LCO.

In order to shed light on these surprising phenomena indicated above, information about the SEI layer on NG and LCO after 15 cycles was obtained with XPS (**Figure 4**) and TOF-SIMS (**Figure 5**). Figure 4a and 4b summarize the XPS results from NG and LCO electrodes, respectively, before (pristine) and after cycling. Two peaks at ~75.3 eV for Al 2p and ~532.4 eV for O 1s in the pristine *c*-NG in Figure 4a clearly confirm the presence of the Al_2O_3 ALD layer. Unexpected signals appear at ~286.2 eV for C 1s ('&') and ~686 eV for F 1s ('$') in the pristine *c*-NG. The former may be indicative of a chemical interaction between Al_2O_3 ALD species and carbon in the NG or PVDF binder. Considering that the latter is slightly negatively-shifted from conventional PVDF, it is most likely attributed to PVDF that was altered by reaction with the ALD coating. This

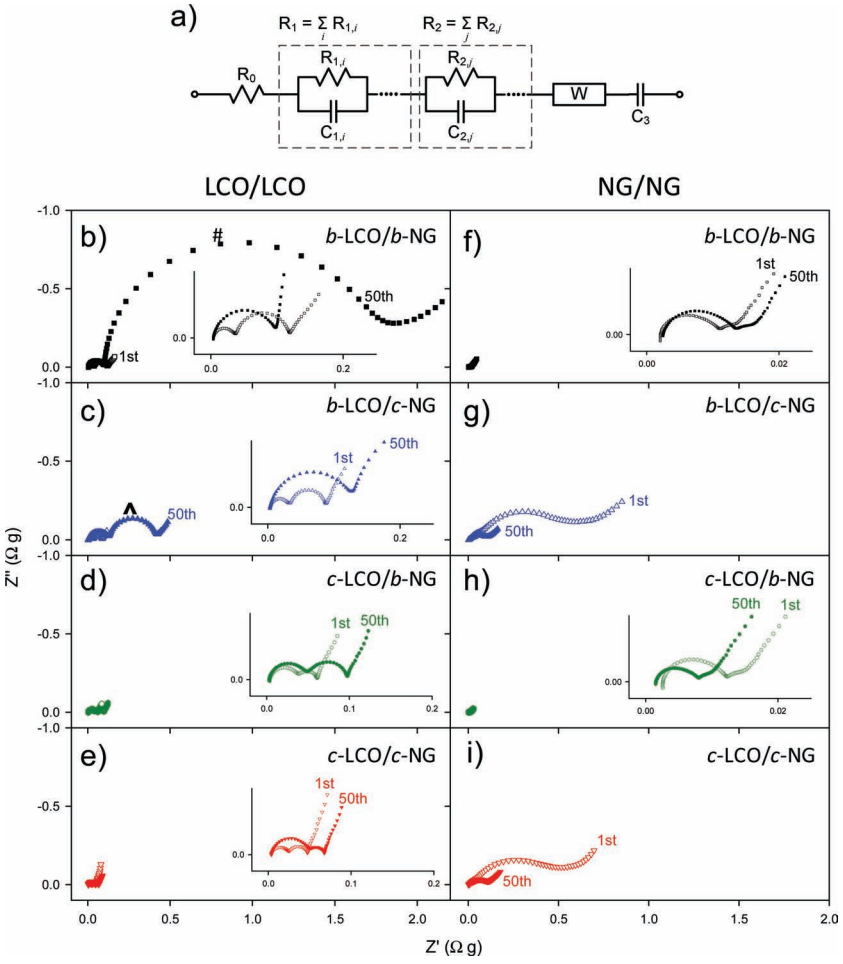

Figure 3. Electrochemical impedance spectroscopy analyses using cycled symmetric cells (SCs). (a) Equivalent circuit model. (b-i) Nyquist plots of LCO/LCO (b-e) and NG/NG (f-i) SCs after the 1st charge and 50th charge. The scale is the same in all plots for each column. Enlarged views are provided in the insets.

is also supported by the disappearance of the PVDF peak at 290.9 eV, C 1s, and the appearance of a weak broad peak shifted by ~ −1 eV. There are also signatures from Li_2CO_3, $ROCO_2Li$, LiF, Li_2O, and–OH, which are commonly observed components in the SEI.[28–30] Among various differences of the signals between the cycled *c*-NG and cycled *b*-NG, it is noticeable that the cycled *c*-NG does not show the Li_2CO_3 peak at ~290.3 eV, C 1s ('♦' in Figure 4a), which is clearly observed for the cycled *b*-NG. This indicates that the ALD coating reduces SEI side reactions on the negative electrode. Overall, the analyses of XPS signals from NG suggest that *c*-NG has a different SEI compared to that of *b*-NG. Surprisingly, however, in analyzing the *b*-LCO (Figure 4b) some unexpected results occur for the *b*-LCO/*c*-NG cell. First, the LiF peak at ~685 eV, F 1s ('◊'), is very intense for *b*-LCO/*b*-NG while it is negligible for *b*-LCO/*c*-NG. Since LiF has very poor Li-ion conductivity, it is believed that the formation of LiF leads to very rapid degradation of the *b*-LCO positive electrode.[28,30] Second, the overall shape of the O 1s spectra for *b*-LCO/*b*-NG is quite different from that for *b*-LCO/*c*-NG, which reflects a different composition of the O-related SEI components. These significant differences in the SEI components on *b*-LCO may partially explain the better durability of *b*-LCO paired with *c*-NG in contrast to *b*-LCO paired with *b*-NG.

To gain even more understanding, depth profiles of the cycled NGs and LCOs with TOF-SIMS are shown in Figure 5a and 5b, respectively, and provide information on the composition *vs.* thickness of the SEI components. For NG electrodes (Figure 5a), Al^+ signals and others (Li_2O^+, Li_2F^+, CH_3^+) are attributed to the Al_2O_3 ALD and inorganic (Li_2O^+, Li_2F^+)/organic(CH_3^+) components of the SEI, respectively. Two dramatic differences between *b*-NG and *c*-NG are noticeable. First, the thickness of Li_2F^+ on the *b*-NG (~24 nm) is almost twice that of the *c*-NG. Second, CH_3^+ signals are very intense only for the *b*-NG (arrow). Thus the TOF-SIMS results strongly indicate a much thinner SEI layer with a smaller organic component on *c*-NG than on *b*-NG, which corroborates the significantly mitigated side reactions on NG by the coating. The signals for *b*-LCO (Li_2F^+ and CH_3^+, Figure 5b) do not exhibit any pronounced difference between *b*-LCO/*b*-NG and *b*-LCO/*c*-NG. This observation most likely indicates that the SEI thickness is not the factor governing degradation of the *b*-LCO. Overall, the differences in both the organic and inorganic NG surface species detected by both the XPS (Figure 4a) and the TOF-SIMS data (Figure 5a) likely play a significant role in the stability of the opposite electrode, *b*-LCO. Finally, TOF-SIMS ions maps of the *b*-LCO electrode from the cycled *b*-LCO/*c*-NG in **Figure 6** show the presence of Al^+ nearby Co^+, indicating Al-species cover the $LiCoO_2$ surface. We suggest that partially reduced Li-Al-O on NG is dissolved by HF, forming soluble Al-containing species that reach the *b*-LCO. This data directly indicates that surface reactions that occur on the negative electrode and positive electrode are related.

It should be noted that side reactions include formation of not only the insoluble SEI components but also soluble byproducts[5,28] such as ROLi, radicals, etc. and even gaseous species. From all the results, which strongly suggest interactions of side reactions between the positive electrode and negative electrode, we propose that soluble byproducts formed by a reductive decomposition reaction on the NG (negative electrode) diffuse to the *b*-LCO (positive electrode), where they again participate in side reactions as depicted by the schematic in **Figure 7**. The movement of the Al species (Figure 6) corroborates this mechanism. Thus, we believe that thicker SEI films with more organic species on *b*-NG imply that more soluble byproducts are formed as well. Coating the NG appears to reduce the formation of soluble byproducts, mitigating the coupled side reaction that accelerates the degradation of the positive electrode (*b*-LCO, Figure 1). Also the Al-species that migrate from the negative electrode to the positive electrode may also contribute to

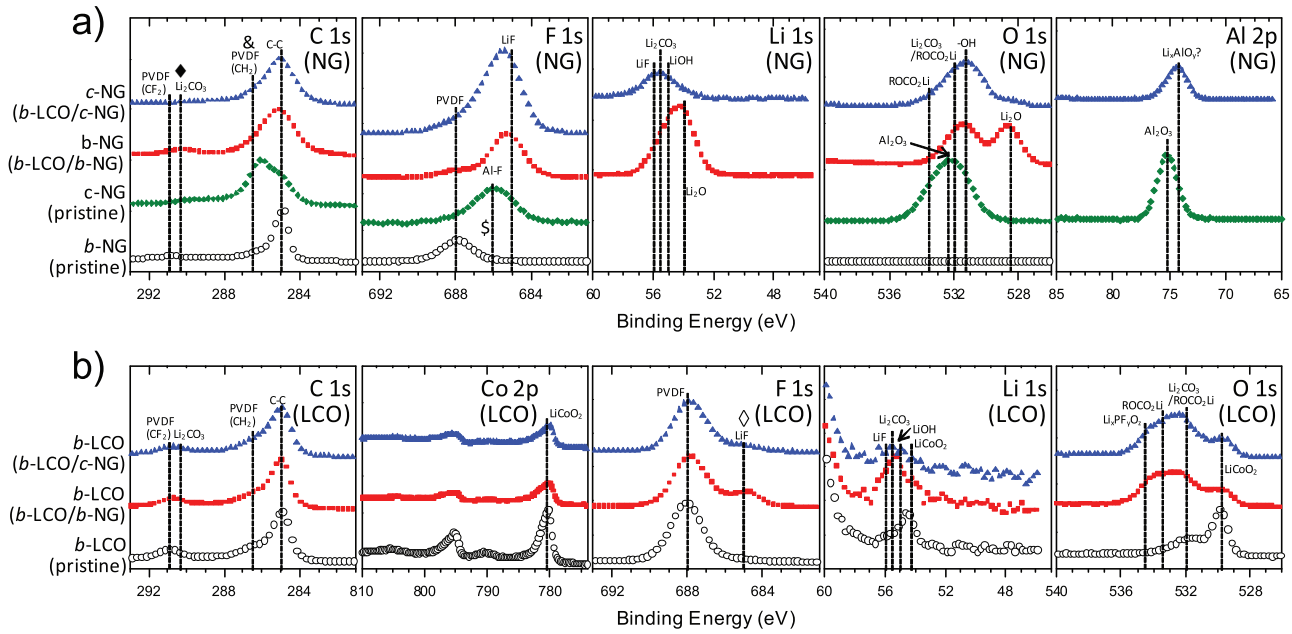

Figure 4. Ex-situ XPS analyses of NG (bare and coated) and bare LCO electrodes before and after charge and discharge cycling: (a) bare and coated NG for the pristine electrodes and after 15 cycles as well as (b) bare LCO for the pristine electrodes and after 15 cycles. Note the significantly reduced intensities of the Li_2CO_3 signal of the cycled *c*-NG as compared to that of the cycled *b*-NG ('♦') and the LiF signal of the cycled *b*-LCO from *b*-LCO/*c*-NG compared to that from *b*-LCO/*b*-NG ('◊').

reducing some of the undesirable side reactions on *b*-LCO by possibly providing a protective layer.

3. Conclusion

The abnormal behavior of significantly superior performance of *b*-LCO/*c*-NG batteries to that of *b*-LCO/*b*-NG was observed even though it is the *b*-LCO that is cycled under harsh conditions. The surface reactions that occur on the negative electrode and positive electrode appear to be related, and this interaction has a very interesting impact on the FC performance. We thus believe our finding may provide a new approach for controlling and designing interfaces in next-generation LIBs. Importantly, the work suggests the possibility of employing coatings to actually tailor surface side reactions that will be the subject of future work.

4. Experimental Section

Al_2O_3 ALD on LCO and NG electrodes: Al_2O_3 ALD films were grown directly on fully fabricated LCO and NG electrodes. For the Al_2O_3 ALD, trimethylaluminum (TMA) (97%) and HPLC (high performance liquid chromatography) grade H_2O were obtained from Sigma-Aldrich. For the TMA/NO_2 nucleation treatment, commercial purity grade NO_2 (99.5%) was acquired from Airgas. The typical growth rate for the chemistry is 1.1 Å per cycle. Also detailed ALD reaction sequences have been described in previous reports.[7,8]

Electrochemical characterization: The LCO composite electrode was prepared by spreading $LiCoO_2$ powder (7-10 µm, L106, LICO Technology), carbon black (CB, super C65, TIMCAL Ltd.), and PVDF (poly(vinylidene fluoride), binder, Kynar) (83.0:7.5:9.5 weight ratio) on a piece of Al foil. The NG composite electrodes were composed of NG (~5 µm, HPM850, Asbury Graphite Mills Inc.) and PVDF (88.9:11.1 weight ratio) on Cu foil. Cells were assembled in an Ar-dry box and tested at room temperature. Based on the mass ratio of LCO/NG in the LCO/NG full cells (~1.60–1.70) and the reversible capacities from the half cell results (LCO/Li: ~185 mA h g^{-1} at 0.1C between 3.3-4.5 V, NG/Li:

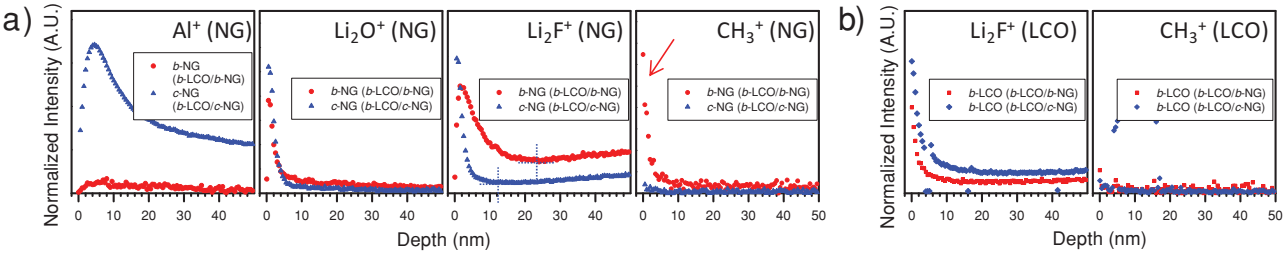

Figure 5. *Ex-situ* TOF-SIMS depth profiling of bare and coated NG (a) and bare LCO (b) after the 15th charge. Note the thinner layers of Li_2F^+ on the cycled *c*-NG compared to the cycled *b*-NG and much stronger signal of CH_3^+ on the cycled *b*-NG than that of the cycled *c*-NG. LCO/NG cells were cycled between 3.25-4.45 V at 0.1C at room temperature prior to the *ex-situ* XPS and TOF-SIMS measurements.

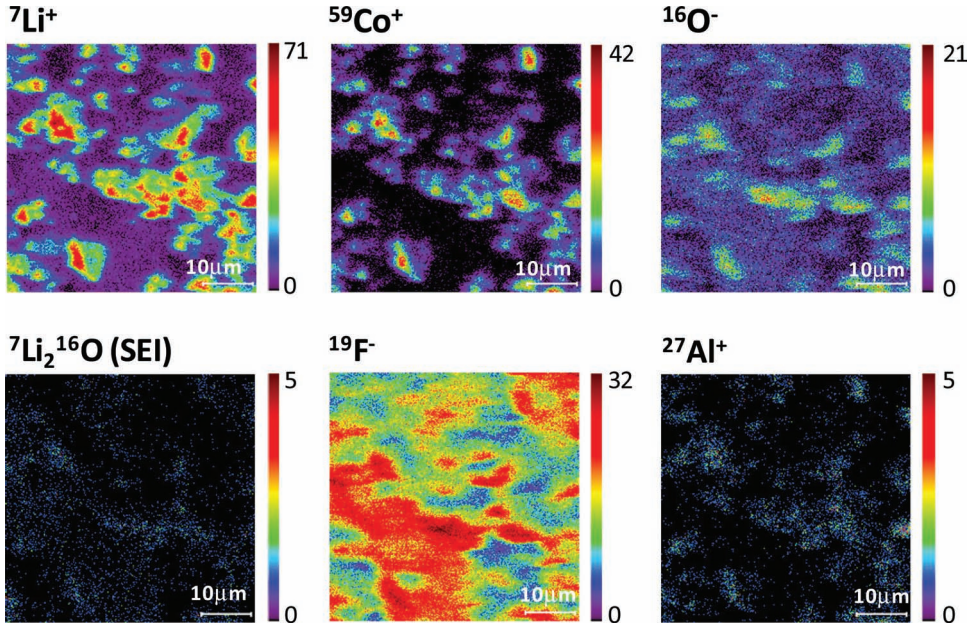

Figure 6. Ex-situ TOF-SIMS ion maps of bare LCO electrodes from the b-LCO/c-NG cell after 15 cycles. Scale bars with the maximum ion counts are displayed in the right of each signal. Note the clear presence of Al-species. LCO/NG cells were cycled between 3.25–4.45 V at 0.1C at room temperature prior to the ex-situ XPS and TOF-SIMS measurements.

~370 mA h g^{-1} at 0.1C between 0.005-1.500 V), np ratio (capacity ratio of NG/LCO) was ~1.2-1.3. The galvanostatic charge-discharge cycling was performed in 2032-type coin cells. 1.0 M $LiPF_6$ dissolved in a mixture of ethylene carbonate (EC) and diethyl carbonate (DEC) (1:1 v/v) (Novolyte Technologies Inc.) was employed as the electrolyte. As the separator, a porous 20 μm thick polypropyl ene (PP)/polyethylene/PP trilayer film (2325, Celgard) was used. Beaker-type cells were assembled for the LCO/Li/NG three electrode assemblies. As depicted in Figure S1, a tiny piece of Li metal (~2 mm in diameter) was connected to a Mo wire (current collector) and placed in between the LCO and NG electrodes separated by the polymer separator. The galvanostatic charge-discharge cycling of the LCO/Li/NG cells was performed by applying current between the LCO and NG electrodes and recording the potential difference between

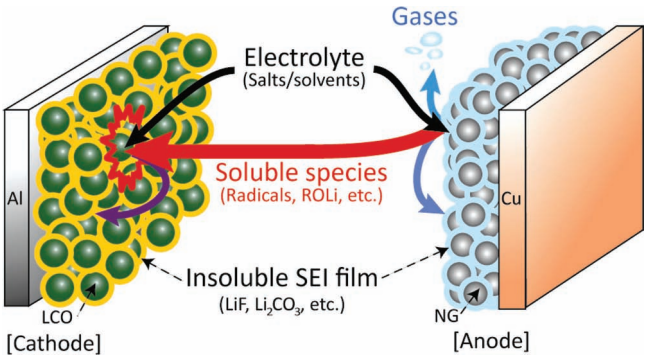

Figure 7. Proposed mechanism of the "coupled side reaction" importantly unraveling the improvement of an LCO/NG battery when only the NG is coated. The soluble byproducts formed by a reductive decomposition reaction on the NG (negative electrode) diffuse to the *b*-LCO (positive electrode) electrode, where they again participate in side reactions. The coating on the NG, thus, likely reduces the formation of soluble byproducts, mitigating the coupled side reaction that accelerates the degradation of *b*-LCO.

LCO and Li. The potential of NG *vs.* Li/Li^{+} was obtained by subtracting the potential of the LCO/NG from that of LCO/Li. The electrochemical impedance spectroscopy (EIS) study was performed using a 1280 C Solartron instrument. The AC impedance measurements were recorded using the SCs with OCP (open circuit potential) of 0 V using a signal with an amplitude of 5 mV and a frequency range from 500 kHz to 5 mHz. The data of the LCO/NG cells at the 1st charge was acquired by charging up to 4.45 V at 0.1C. Another set was obtained by cycling at 0.1C between 3.25–4.45 V for the first two cycles and at 1C for the next 47 cycles, then charging up to 4.45 V at 0.1C for the 50th charge. After resting for >6 h, the cycled LCO/NG cells were disassembled, the collected LCO and NG electrodes were separated and reassembled as LCO/LCO and NG/NG symmetric cells with the same electrolyte (1 M $LiPF_6$ in a mixture of EC and DEC) as the case of LCO/NG FCs inside a glove box.

Ex-situ surface analyses: Characterization with XPS was performed using a PHI 5600 X-ray photoelectron spectrometer with a monochromatic Al K_{α}asource (1486.6 eV). The base pressure in the XPS analysis chamber was 5×10^{-8} Pa. XPS spectra were collected using a constant analyzer energy mode with a pass energy between 58.7-93.9 eV. The step size was varied between 0.25-0.4 eV. TOF-SIMS analyses were conducted on a PHI TRIFT V nanoTOF (Physical Electronics, Chanhassen, MN). A 30 kV Au^{+} source was employed for analysis and sputtering. The TOF-SIMS imaging areas were 50×50 μm^2. The depth profiles were collected from a 50×50 μm^2 area inside a 200×200 μm^2 sputtering area. The base pressure of the analysis chamber was maintained at $<2.5 \times 10^{-7}$ Pa during all analyses. For the ex-situ XPS and TOF-SIMS analyses, the LCO/NG cells were charged-discharged between 3.25–4.45 V at 0.1C for 15 cycles at room temperature. After the LCO/NG cells were disassembled, the electrodes were collected, soaked in DEC for ~1 h, and dried inside a glove box. For the XPS measurements, the electrode samples were transported using hermetically sealed glass jars and exposed to atmosphere for <1 min before mounting in the XPS. For the TOF-SIMS measurement, after the hermetically sealed samples were transported, the samples were directly transferred from an Ar filled glove box to the TOF-SIMS for analysis. During the transfer process, samples were kept under Ar atmosphere in an air-tight transfer vessel to avoid all contact with air.

Supporting Information

Supporting Information is available from the Wiley Online Library or from the author.

Acknowledgements

This work was supported by the U.S. Department of Energy under Contract No. DE-AC36-08-GO28308 through: the NREL Director's Research and Development Program within the National Renewable Energy Laboratory as well as through the DOE EERE VT BATT program. This research was also supported by Energy Efficiency and Resources R&D program (20112010100150) and by the ITRC (Information Technology Research Center) support program (NIPA-2012-H0301-12-1009) supervised by the NIPA (National IT Industry Promotion Agency) under the MKE (The Ministry of Knowledge Economy), Korea, and by a grant from Creativity and Innovation Project funded by the UNIST (Ulsan National Institute of Science and Technology) (1.120027.01). We thank A. Pesaran and T. Penny for NREL program/project guidance, G. Teeter for experimental assistance and valuable discussions and K. J. Lee for assisting in the schematic diagram.

Received: May 24, 2012
Revised: July 3, 2012
Published online: September 13, 2012

[1] M. Armand, J.-M. Tarascon, *Nature* **2008**, *451*, 652.
[2] J. B. Goodenough, Y. Kim, *Chem. Mater.* **2010**, *22*, 587.
[3] A. C. Dillon, *Chem. Rev.* **2011**, *110*, 6856.
[4] Idaho National Laboratory website, Battery Test Manual for Plug-In Hybrid Electric Vehicle; http://www.inl.gov (accessed August 2012).
[5] D. Aurbach, *J. Power Sources* **2000**, *89*, 206.
[6] T. Doi, L. Zhao, M. Zhou, S. Okada, J. Yamaki, *J. Power Sources* **2008**, *185*, 1380.
[7] Y. S. Jung, A. S. Cavanagh, A. C. Dillon, M. D. Groner, S. M. George, S. H. Lee, *J. Electrochem. Soc.* **2010**, *157*, A75.
[8] Y. S. Jung, A. S. Cavanagh, L. A. Riley, S. H. Kang, A. C. Dillon, M. D. Groner, S. M. George, S. H. Lee, *Adv. Mater.* **2010**, *22*, 2172.
[9] K. Xu, *Chem. Rev.* **2004**, *104*, 4303.
[10] J. Cho, Y. J. Kim, T. J. Kim, B. Park, *Angew. Chem. Int. Ed.* **2001**, *40*, 3367.
[11] J. Cho, Y. W. Kim, B. Kim, J. G. Lee, B. Park, *Angew. Chem. Int. Ed.* **2003**, *42*, 1618.
[12] C. Li, H. P. Zhang, L. J. Fu, H. Liu, Y. P. Wu, E. Rahm, R. Holze, H. Q. Wu, *Electrochim. Acta* **2006**, *51*, 3872.
[13] I. Scott, Y. S. Jung, A. S. Cavanagh, Y. Yan, A. C. Dillon, S. M. George, S. H. Lee, *Nano Lett.* **2011**, *11*, 414.
[14] L. A. Riley, A. S. Cavanagh, S. M. George, Y. S. Jung, Y. Yan, S. H. Lee, A. C. Dillon, *ChemPhysChem* **2010**, *11*, 2124.
[15] E. Kang, Y. S. Jung, A. S. Cavanagh, G. H. Kim, A. C. Dillon, S. M. George, J. K. Kim, J. Lee, *Adv. Funct. Mater.* **2011**, *21*, 2430.
[16] Y. S. Jung, A. S. Cavanagh, L. Gedvilas, N. E. Widjonarko, I. D. Scott, S.-H. Lee, G.-H. Kim, S. M. George, A. C. Dillon, *Adv. Energy Mater.* **2012**,*2*, 1022.
[17] Y. He, X. Yu, Y. Wang, H. Li, X. Huang, *Adv. Mater.* **2011**, *23*, 4938.
[18] Y. Liu, N. S. Hudak, D. L. Huber, S. J. Limmer, J. P. Sullivan, J. Y. Huang, *Nano Lett.* **2011**, *11*, 4188.
[19] A. C. Dillon, A. W. Ott, J. D. Way, S. M. George, *Surf. Sci.* **1995**, *322*, 230.
[20] S. M. George, *Chem. Rev.* **2010**, *110*, 111.
[21] J. Christensen, J. Newman, *J. Electrochem. Soc.* **2005**, *152*, A818.
[22] D. H. Jang, Y. J. Shin, S. M. Oh, *J. Electrochem. Soc.* **1996**, *143*, 2204.
[23] I. H. Cho, S. S. Kim, S. C. Shin, N. S. Choi, *Electrochem. Solid-State Lett.* **2010**, *13*, A168.
[24] D. B. Farmer, R. G. Gordon, *Nano Lett.* **2006**, *6*, 699.
[25] P. Ramadass, B. Haran, R. White, B. N. Popov, *J. Power Sources* **2002**, *111*, 210.
[26] M. Gaberscek, J. Moskon, B. Erjavec, R. Dominko, R. J. Jamnik, *Electrochem. Solid-State Lett.* **2008**, *11*, A170.
[27] E. Kang, Y. S. Jung, G. H. Kim, J. Chun, U. Wiesner, A. C. Dillon, J. K. Kim, J. Lee, *Adv. Funct. Mater.* **2011**, *21*,4349.
[28] A. Zaban, E. Zinigrad, D. Aurbach, *J. Phys. Chem.* **1996**, *100*, 3089.
[29] D. Aurbach, M. D. Levi, E. Levi, A. Schechter, *J. Phys. Chem. B* **1997**, *101*, 2195.
[30] Y. C. Lu, A. N. Mansour, N. Yabuuchi, Y. Shao-Horn, *Chem. Mater.* **2009**, *21*, 4408.